Electronic Supplementary Material (ESI) for Journal of Materials Chemistry B.

Supporting Information

Core-Shell Nanodiamonds-Periodic Mesoporous Organosilica Nanoparticles for Two-Photon Imaging, Photodynamic Therapy and Synergistic pH-Responsive Drug Delivery.

Chiara Mauriello Jimenez,[a] Nikola Z. Knezevic,[a] Yolanda Galàn Rubio,[a] Sabine Szunerits,[b] Rabah Boukherroub,[b] Florina Teodorescu ,[b] Jonas G. Croissant,[a] Ouahiba Hocine,[a] Martina Seric,[a] Laurence Raehm,[a] Vanja Stojanovic,[c] Dina Aggad,[c] Marie Maynadier,[d] Marcel Garcia,[c] Magali Gary-Bobo[c] and Jean-Olivier Durand[a]

[a]Institut Charles Gerhardt Montpellier,UMR 5253,CC 1701 Equipe Ingénierie Moléculaire et Nano-objets, Place Eugène Bataillon, 34095 Montpellier Cedex 05,France.
[b]Institut d'Electronique, de Microélectronique et de Nanotechnologie (CNRS UMR8520)-Université de Lille 1 – Sciences et Technologies-Parc de la Haute Borne-50 avenue de Halley-59658 Villeneuve d'Ascq
[c]Institut de Biomolécules Max Mousseron, UMR 5247, Avenue Charles Flahault, 34093 Montpellier Cedex 05, France
[d]NanoMedSyn, Faculté de Pharmacie, Avenue Charles Flahault, 34093 Montpellier Cedex 05, France.

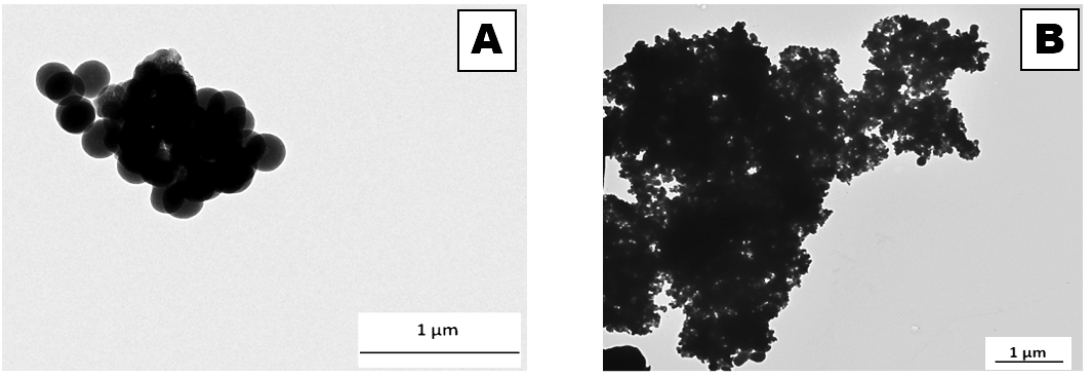

Figure S1. TEM images of ND@ENE (A) and ND@E NPs (B).

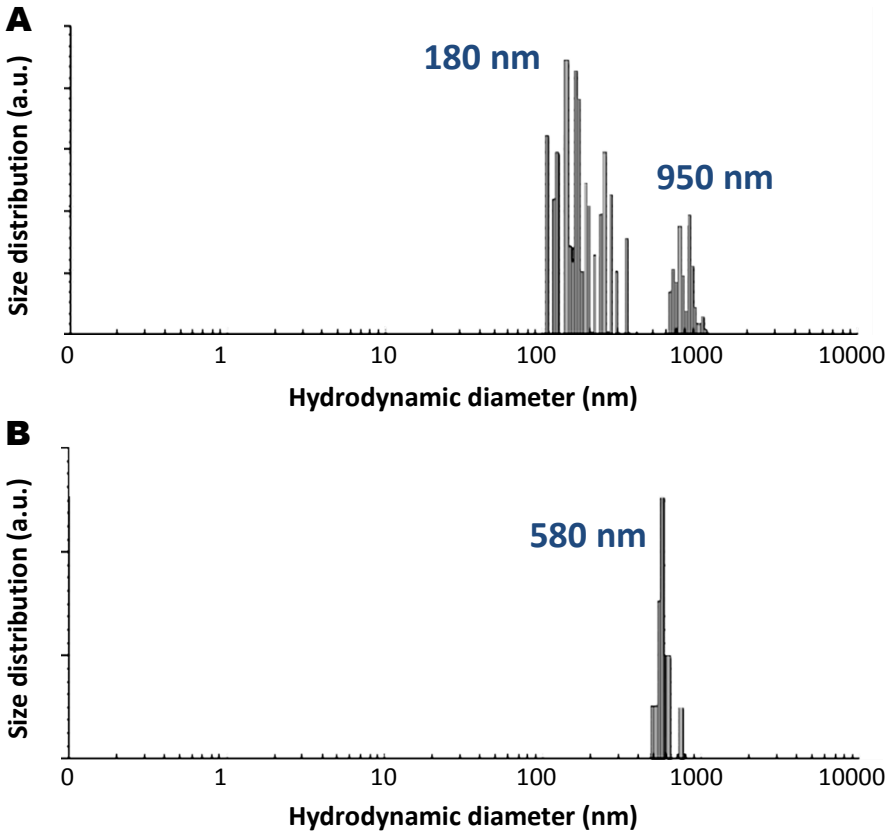

Figure S2. DLS analyses (Intensity) of ND@ENE (A) and ND@E (B).The large diameter arose from the aggregation states of the particles as well as the hydration layers.

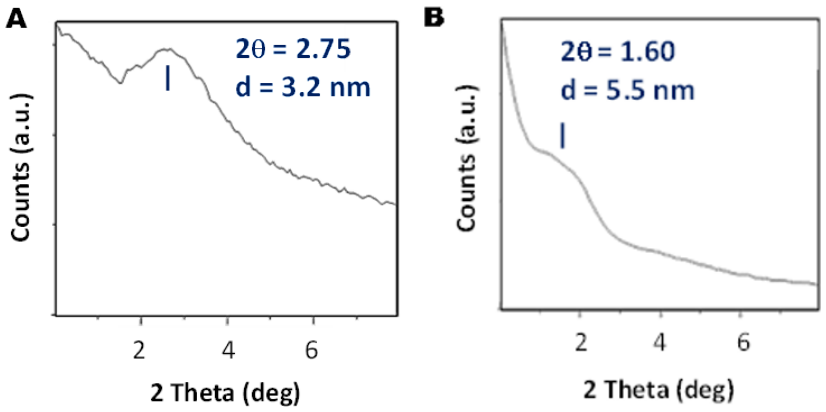

Figure S3. Small angle XRD patterns of ND@ENE (A), ND@E (B), consistent with the porous silsesquioxane frameworks in the materials.

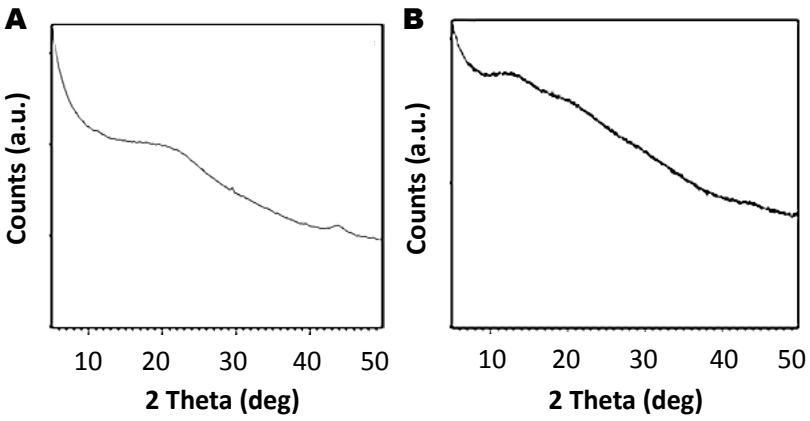

Figure S4. Wide angle XRD patterns of ND@ENE (A), ND@E (B) consistent with the amorphous porous silsesquioxane frameworks.

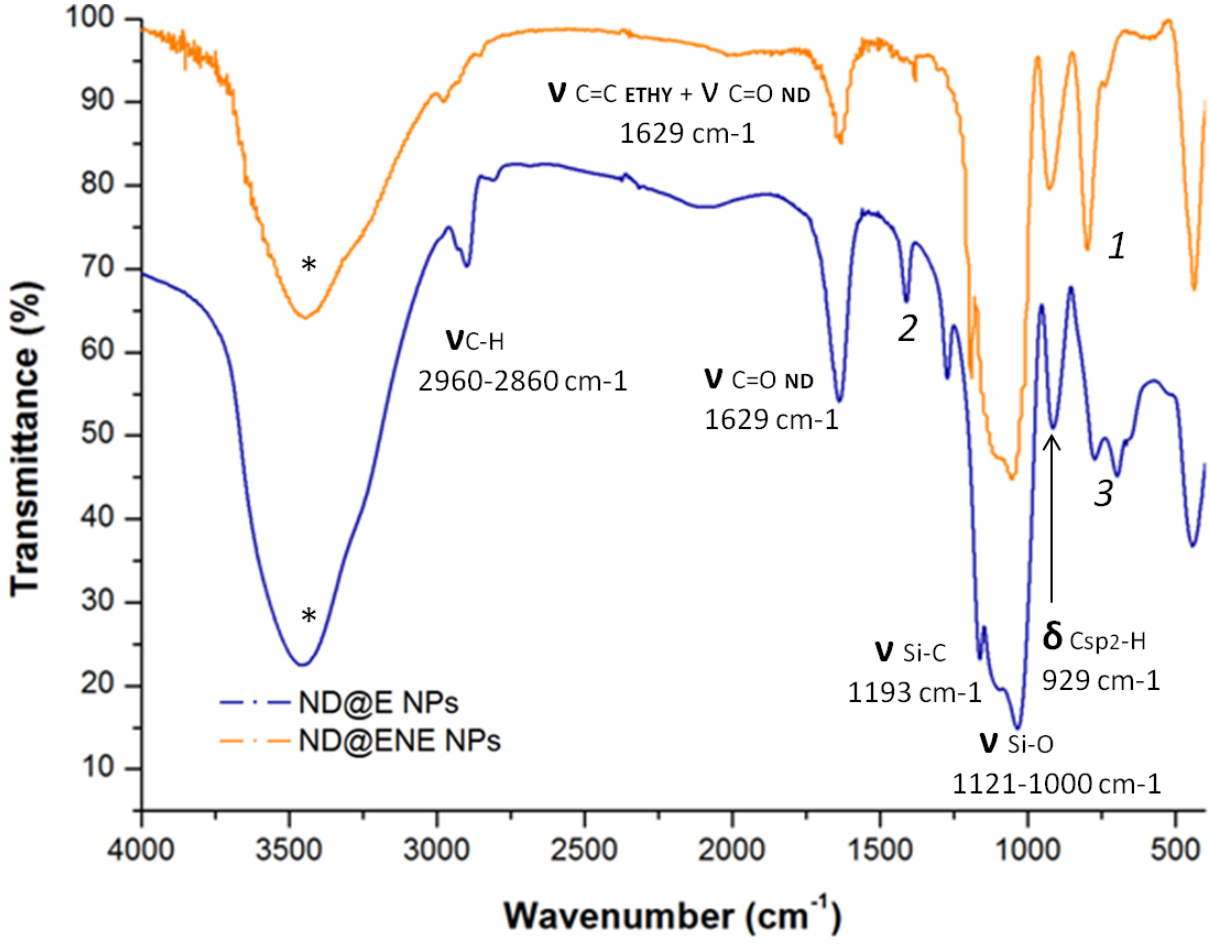

Figure S5. FTIR spectra of ND@ENE NPs and ND@E NPs confirming the presence of the ethylene or ethane and NDs. * Indicates the vibration modes of water. *1* Vibration mode of the ethenylene bridges, likely another $\delta_{Csp2\text{-}H}$. *2* Vibration modes of the ethylene bridges, likely a $\delta_{C\text{-}C}$. *3* Vibration modes of the ethylene bridges, likely other $\delta_{Csp2\text{-}H}$.

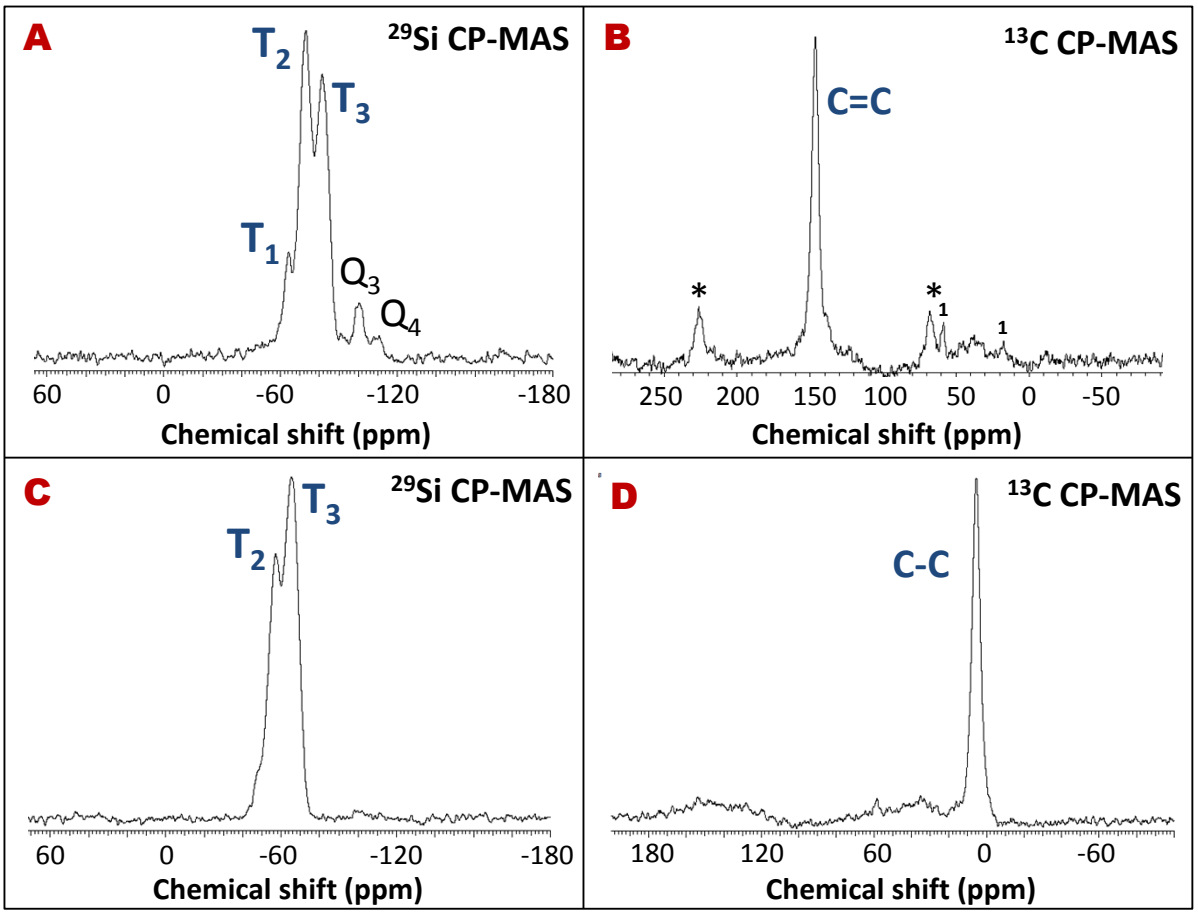

Figure S6. ^{29}Si and ^{13}C Solid state NMR CPMAS spectra of ND@ENE NPs (A-B) and ND@E NPs (C-D). The major proportions of T_2 and T_3 in the silicon spectra correlates a stable silsesquioxane network. The ethenylene and ethylene bridges are clearly distinguished *via* carbon NMR. * Indicates the spinning side bands. *1* remaining Si-O-CH_2-CH_3.

I-TWO-PHOTON *IN-VITRO* STUDIES

TP-imaging. A day prior to the experiment, MCF-7 cells were seeded onto bottom glass dishes (World Precision Instrument, Stevenage, UK) at a density of 10^6 cells cm^{-2}. Adherent cells were then washed once and incubated in 1 mL culture medium containing NPs at a concentration of 40 µg mL^{-1} for 20 h. Fifteen min before the end of incubation, cells were loaded with Cell Mask TM Orange Plasma Membrane Stains (Invitrogen, Cergy Pontoise, France) for membrane staining at a final concentration of 5 µg mL^{-1}. Before visualization, cells were washed gently with phenol red-free DMEM. Cells were then scanned with LSM 780 LIVE (Carl Zeiss, Le Pecq, France), at 750 or 800 nm with a slice depth (Z stack) of 0.62 µm.

TPE-therapy. MCF-7 human breast cancer cells were cultured in Dulbecco's modified Eagle's medium (DMEM) supplemented with 10 % fetal bovine serum and 50 µg mL^{-1} gentamycin. All cells were allowed to grow in humidified atmosphere at 37 °C under 5 % CO_2. For *in vitro* phototoxicity, MCF-7 cells were seeded into a 384 multiwell glass-bottomed plate (thickness 0.17 mm), with a black polystyrene frame, 2000 cells per well in 50 µL of culture medium, and allowed to grow for 24 h. NPs were dispersed under ultrasounds in PBS at a concentration of 1 mg mL^{-1} and cells were then incubated for 5 h with or without nanoparticles at a final

concentration of 80 µg mL^{-1} in supplemented DMEM. After incubation with NPs, cells were washed twice, maintained in fresh culture medium, and then submitted (or not) to laser irradiation. After 2 days, the MTS assay was performed and was corrected.

II-UNLOADED NPS IN-VITRO CONTROL

Cytotoxicity for 72 h. MCF-7 cells were incubated with increasing concentrations of NPs (from 5 to 200 µg mL^{-1}). After 72 h treatment, a MTT assay was performed and data are mean ± SD of 3 experiments.

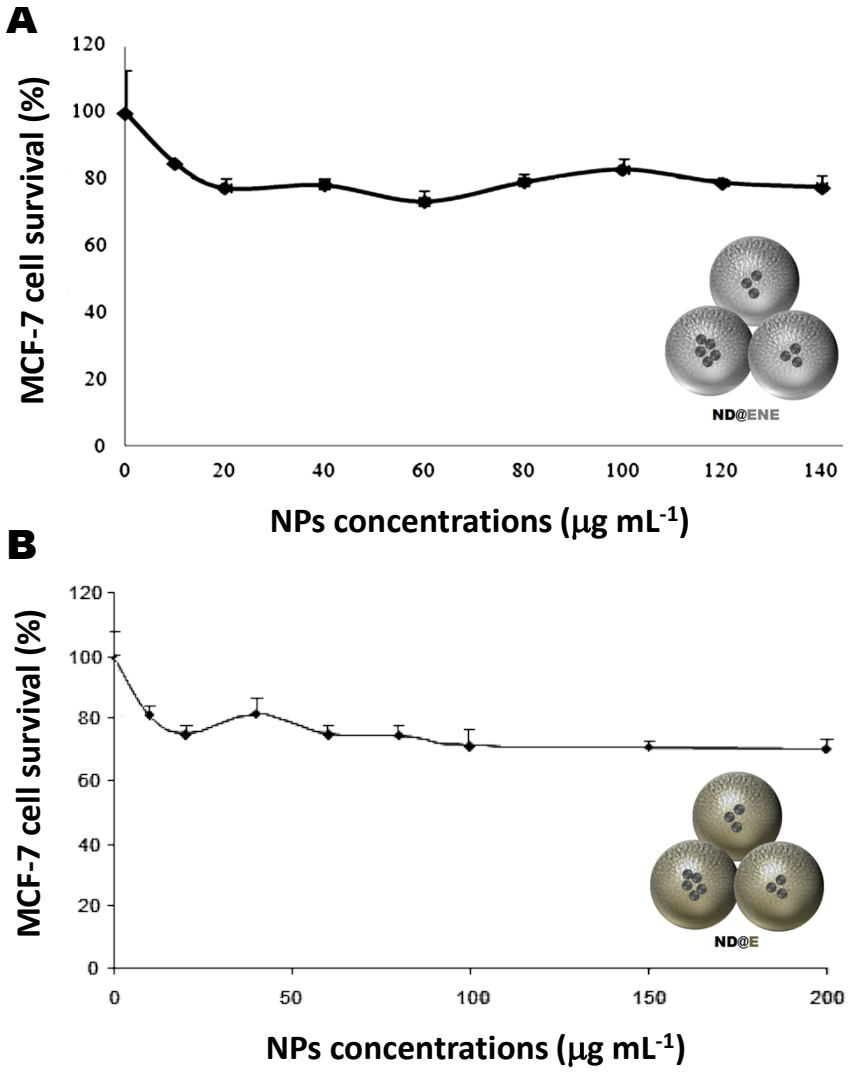

Figure S7. Cytotoxicity of ND@ENE NPs (A) and ND@E NPs (B) on MCF-7 cells after 72 h of incubation.

III – pH responsive drug release.

Release experiment of DOX-loaded ND@E NPs was performed in ultrapure water upon addition, after 60 min, of HCl (0.2 M) to obtain a lysosomal pH.

A

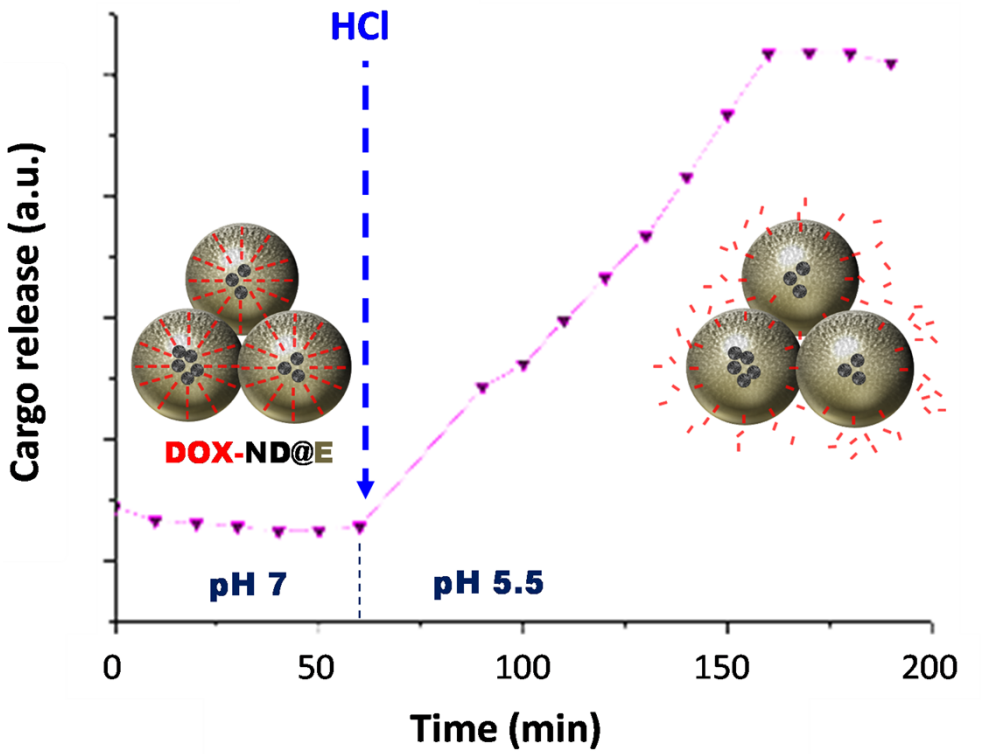

B

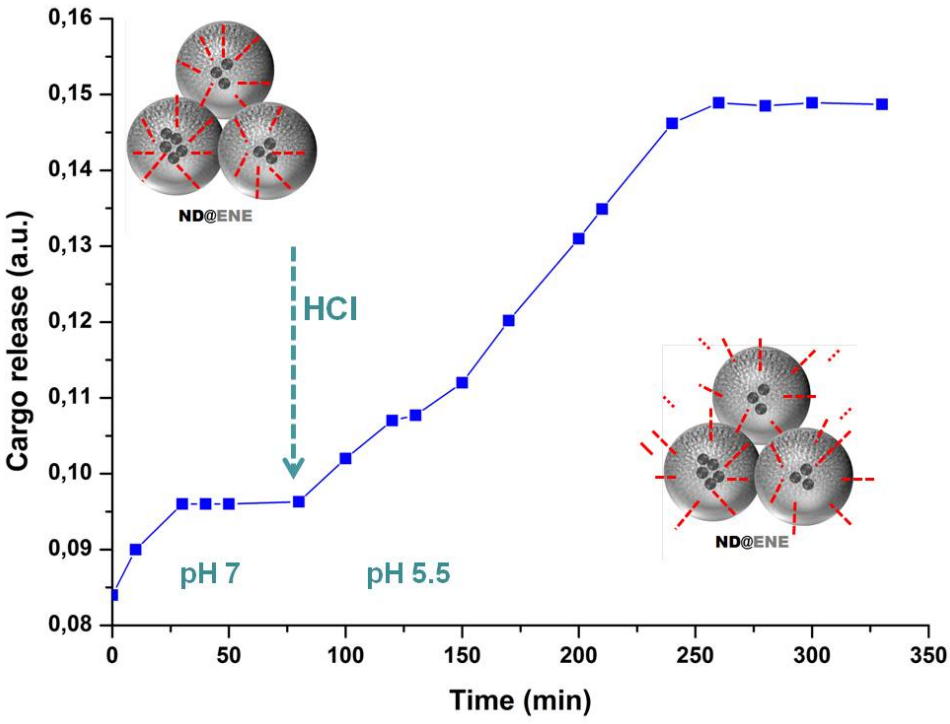

Figure S8. DOX release from DOX-ND@E (A) and DOX-ND@ENE NPs (B) in water upon pH trigger from a neutral condition to pH 5.5.

IV - DRUG DELIVERY EXPERIMENTS

MCF-7 cells were seeded into 96-well plates at 2000 cells per well in 200 µL culture medium and allowed to grow for 24 h. Increasing concentrations of DOX ND@E NPs (from 0.01 to 200 µg mL^{-1}) dispersed in sterile water, were incubated in culture medium of MCF-7 cells during 72 h and a MTT assay was performed to evaluate the toxicity. Briefly, cells were incubated for 4 h with 0.5 mg mL^{-1} of MTT (3-(4,5-dimethylthiazol-2-yl)-2,5-diphenyltetrazolium bromide, Promega). The MTT medium solution was then removed and the precipitated crystals were dissolved in EtOH/DMSO (1:1). The solution absorbance was recorded at 540 nm.

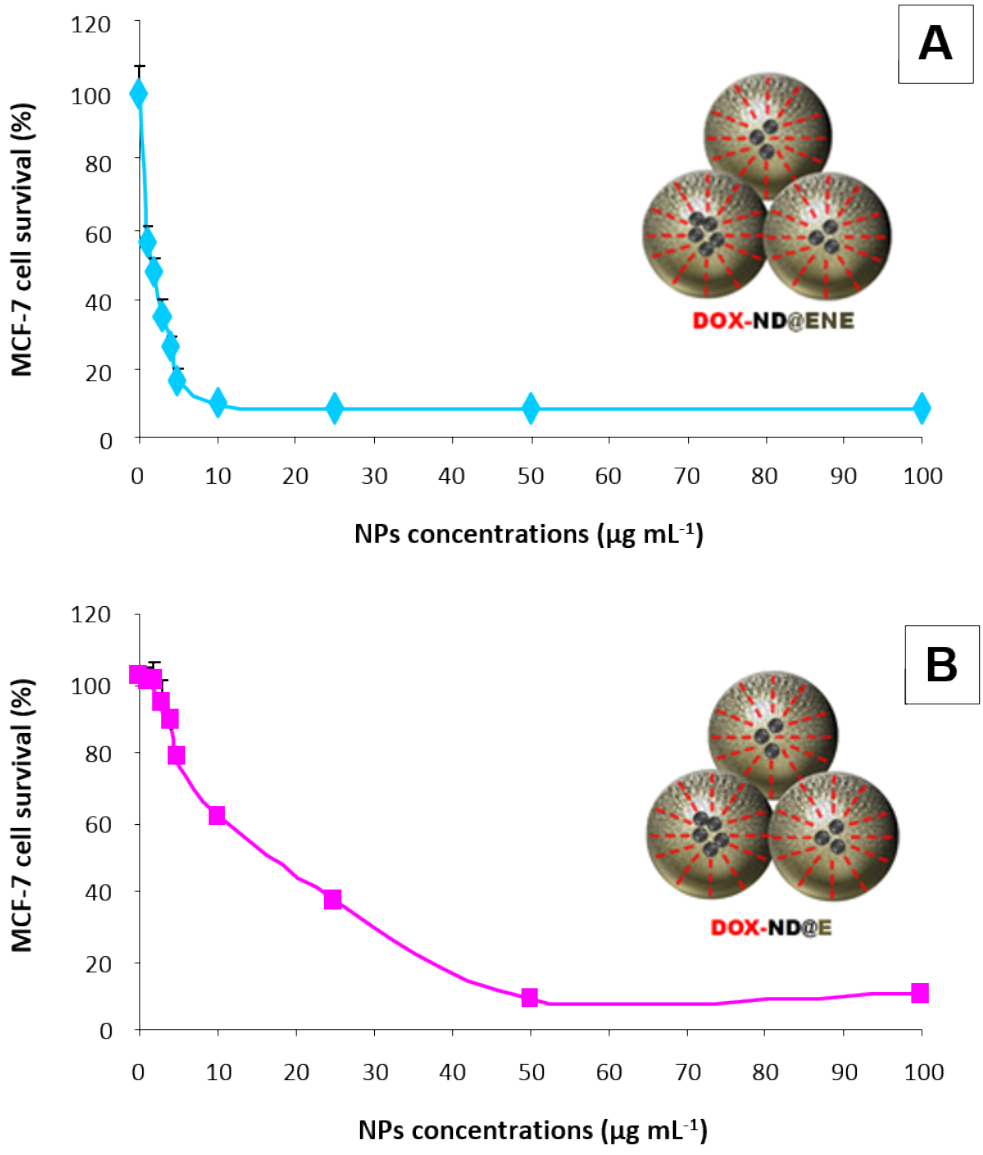

Figure S9. DOX delivery in MCF-7 cancer cells *via* DOX-ND@ENE NPs (A) and DOX-ND@E NPs (B) at 72h of incubation.

V - PHOTOTHERMAL EFFECT

Irradiations were performed in standard 96-well plates with pulsed titanium: saphir laser (Chameleon model, Coherent). This laser source delivers 100 fs pulses at a repetition rate of 80 MHz and was used for the photothermal experiments. A telescope with a magnification of 4.3 is used to roughly adapt the beam diameter to the wells' one. The beam diameter was previously measured with a Thorlabs DCU224C CCD camera (New Jersey, USA) and the variation in the diameter over the wavelength along with the setup efficiency was corrected with the laser average power in the calculation of the applied intensity. The wavelength used was 810 nm with

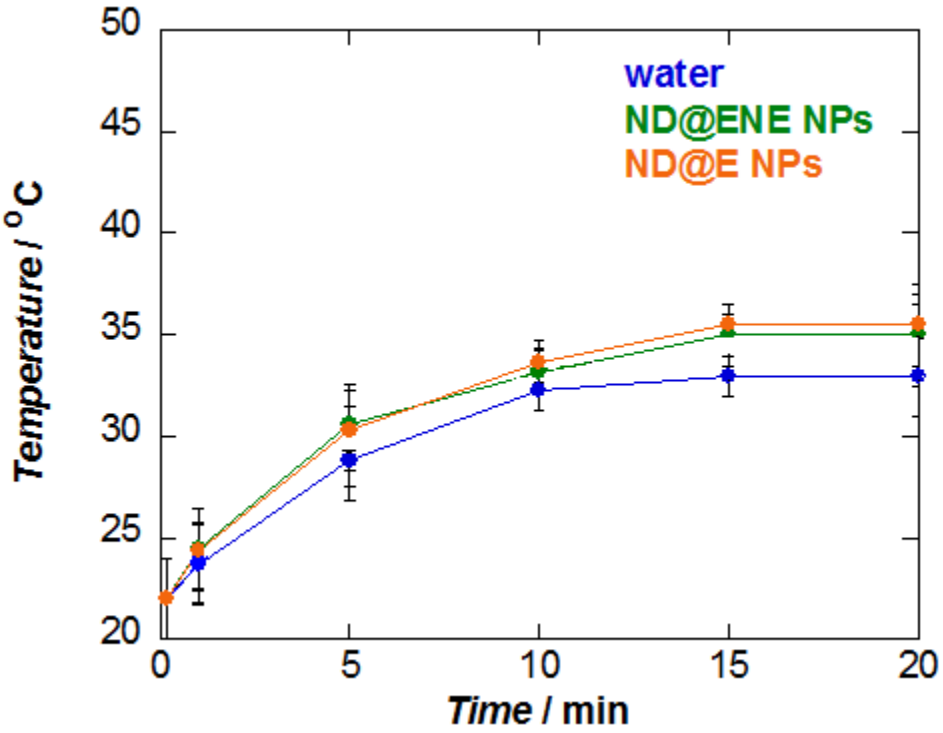

the laser power intensity of 1 W cm^{-2}. The temperature change was captured by Infrared Camera (Thermovision A40, FLIR system, USA) and treated using the ThermaCam Researcher Pro 2.9 software.

Figure S10. Photothermal effect of the pulsed irradiation for two-photon-excitation of ND@E, ND@ENE NPs, (100 µg.mL^{-1} in water) and a water solution control.

VI – ROS IMAGING

The detection of intracellular reactive oxygen production (ROS) was realized using DCFDA Cellular ROS Detection Assay Kit (abcam). For this, MCF-7 cells were seeded in glass bottom microplate and treated with 80

µg mL^{-1} nanoparticles. After 24 h, cells were rinsed and incubated 45 min at 37 °C with DCFDA at 20 µM. Then, cells were rinsed and irradiated or not with a two-photon microscope (3 x 1.57 sec) at 800 nm. Green luminescence traduces the generation of ROS detected at 535 nm.

VII – CONTROL EXPERIMENTS WITH ENE PMO NPs without NDs.

The 2PE-PDT efficacy and the ROS production were verified by using ENE PMO NPs without ND. The experimental conditions used for TPE-PDT and ROS production are the same as those already used.

The results presented in figures S12 and S13 show that nor PDT effect neither ROS production was observed with ENE PMO . This demonstrate that the biological effects with ND@PMO are due to ND.

Figure S11. TPE-PDT with PMO alone in MCF-7 cells. Cells were incubated 20 h with ENE PMO at the concentration of 80 µg.mL^{-1}. TPE was performed 3 x 1.57 sec at 800 nm.

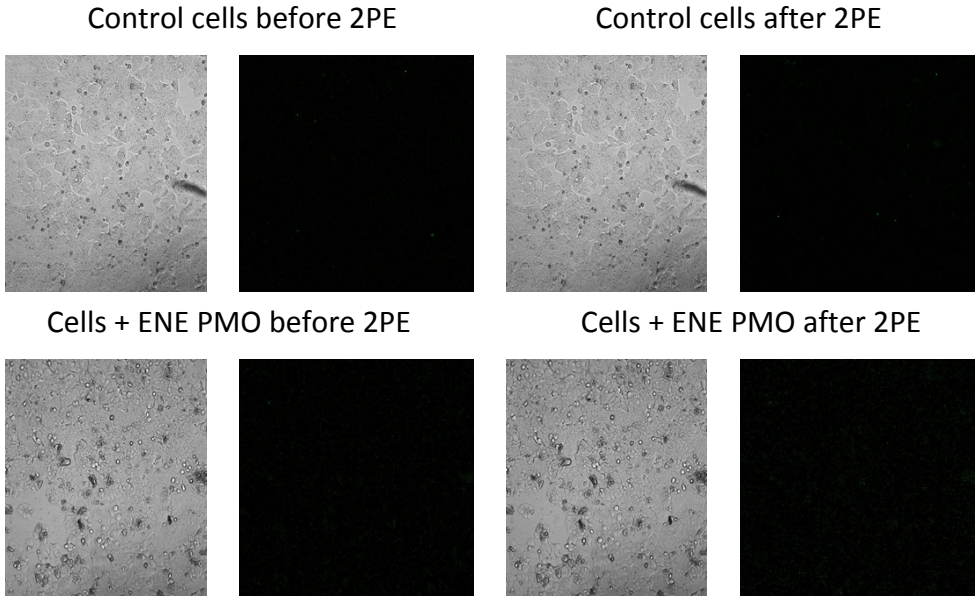

Figure S12. ROS analysis by DCFDA in MCF-7 cells. Cells were incubated for 24 h with ENE PMO at the concentration of 80 µg.mL^{-1} and submitted to laser irradiation 3 x 1.57 sec at 800 nm.

VIII – TPE EXPERIMENTS WITH NDs WITHOUT THE PMO shell.

Cytotoxic study of NDs

To investigate the biocompatibility of diamond nanoparticles, increasing concentrations (from 5 to 140 µg.mL^{-1}) of diamond nanoparticles were incubated in culture medium of MCF-7 cells during 72 h and then the percentage of living cells were evaluated. No significant cell death was observed, demonstrating the diamond nanoparticles biocompatibility *in vitro* (Figure S113).

Cellular uptake of NDs

To evaluate the diamond nanoparticles cellular uptake, 40 µg.mL^{-1} of diamond nanoparticles were incubated for 20 h in MCF-7 breast cancer cells and the cell membranes were stained with Cell Mask Orange. Diamond nanoparticles were readily visible, inside the cytosol, through TPE-fluorescence imaging which demonstrates the successfully endocytosis by cancer cells (Figure S14).

Photodynamic therapeutic potential of the NDs

To confirm that TPE-PDT effect of PMO NPs is due to nanodiamonds, the photo-activable diamond nanoparticles were incubated in culture medium of MCF-7 cells during 20 h at a final concentration of 80 µg.mL^{-1} and the percentage of living cells were evaluated after, or not, laser irradiation. The diamond nanoparticles were found to be non toxic without irradiation and irradiation alone did not damage the cells. A selective cancer cell-killing of 32 ± 6% were observed in the presence of irradiated diamond nanoparticles, clearly proving the diamond nanoparticles photodynamic therapeutic potential (Figure S15).

NDs specifically induce oxidative stress generation in MCF-7 cells.

The capacity of the diamond nanoparticles to generate oxidative stress was analyzed by Dichlorofluorescin diacetate assay on MCF-7 breast cancer cells. MCF-7 cells were incubated for 24 hours at a concentration of 80 µg.mL^{-1} with diamond nanoparticles and then exposed to 20 µM 2', 7'-dichlorofluorescin diacetate (DCFDA) for 45 minutes. Cells were rinsed and imaged before and after laser irradiation. Figure S4bio shows a clear ROS production in cells treated with diamond nanoparticles after laser irradiation. These results confirm that cytotoxicity was produced by the presence of the diamond nanoparticles in PMO NPs under two-photon excitation. (Figure S16).

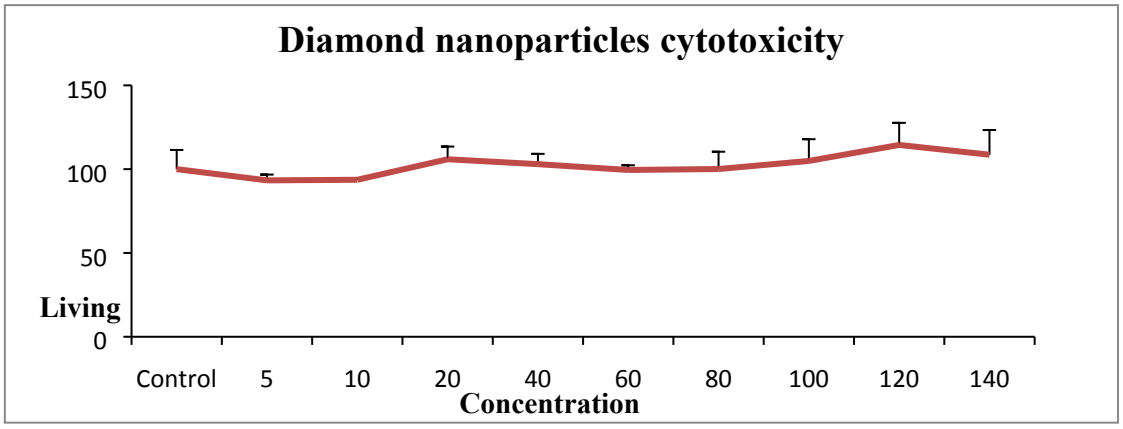

Figure S13. Effect of NDs on MCF-7 cells growth. Increasing concentrations of NDs were incubated in culture medium of MCF-7 cells. After 72 h, a MTT assay was performed to quantify living cells. Data are mean ± standard deviation of three experiments.

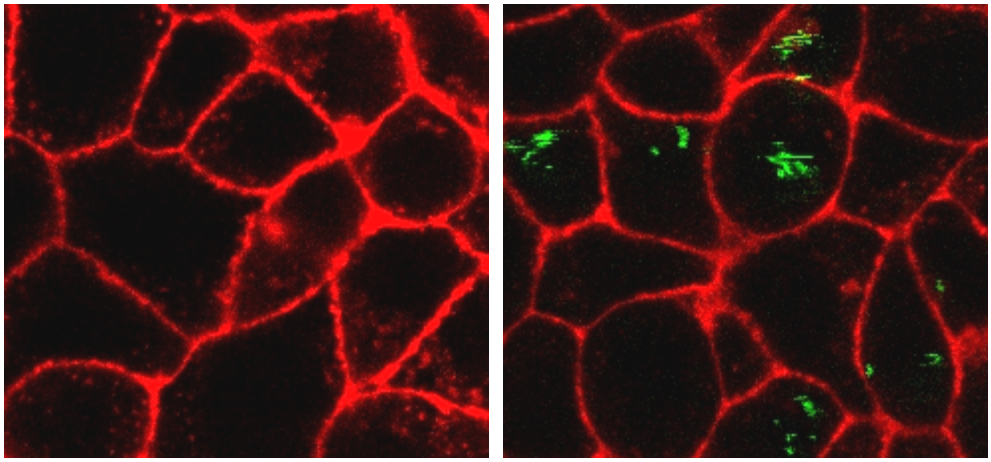

Figure S14. Two-photon fluorescence imaging. Cells were incubated for 20 h with 40 µg mL^{-1} NDs and stained with cell mask for membrane detection in red. NDs imaging was performed at 800 nm.

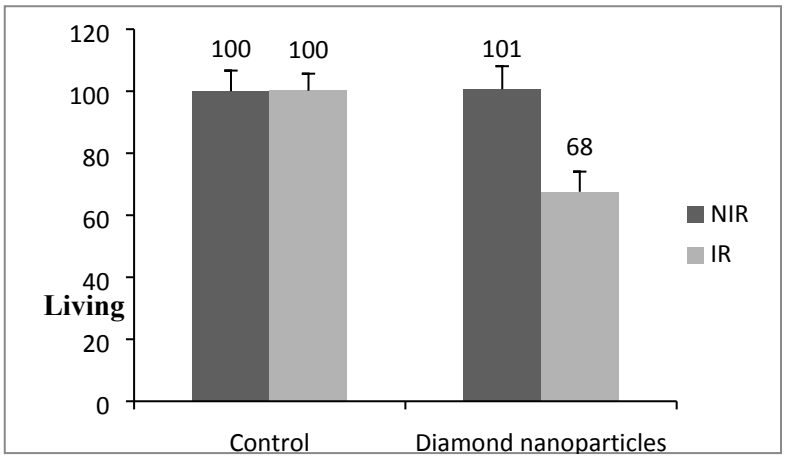

Figure S15. TPE-triggered cancer cell killing of NDs. Cells were incubated 20 h with NDs at the concentration of 80 µg.mL^{-1}. TPE was performed 3 x 1.57 sec at 800 nm. Two days after irradiation, MTT assay was performed to quantify living cells. Data are mean values standard deviation from three independent experiments.

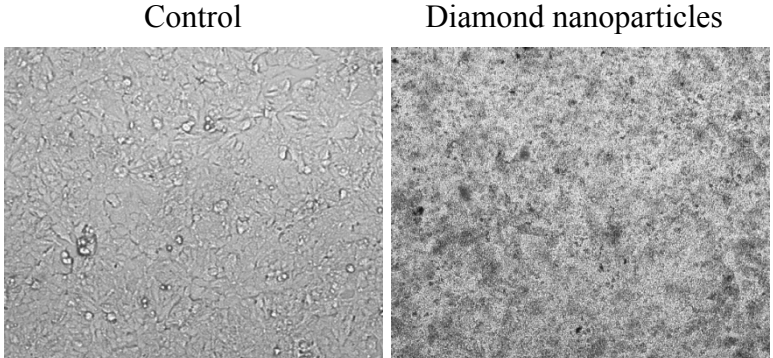

Figure S16. Detection of intracellular ROS by DCFDA assay in MCF-7 cancer cells. Cells were incubated for 24 h with diamond nanoparticles (80 μg.mL^{-1}) and ROS production in cells is induced by TPE (1scan of 1.57 sec) at 800 nm. Green luminescence shows the generation of ROS detected at the wavelength of 535 nm.

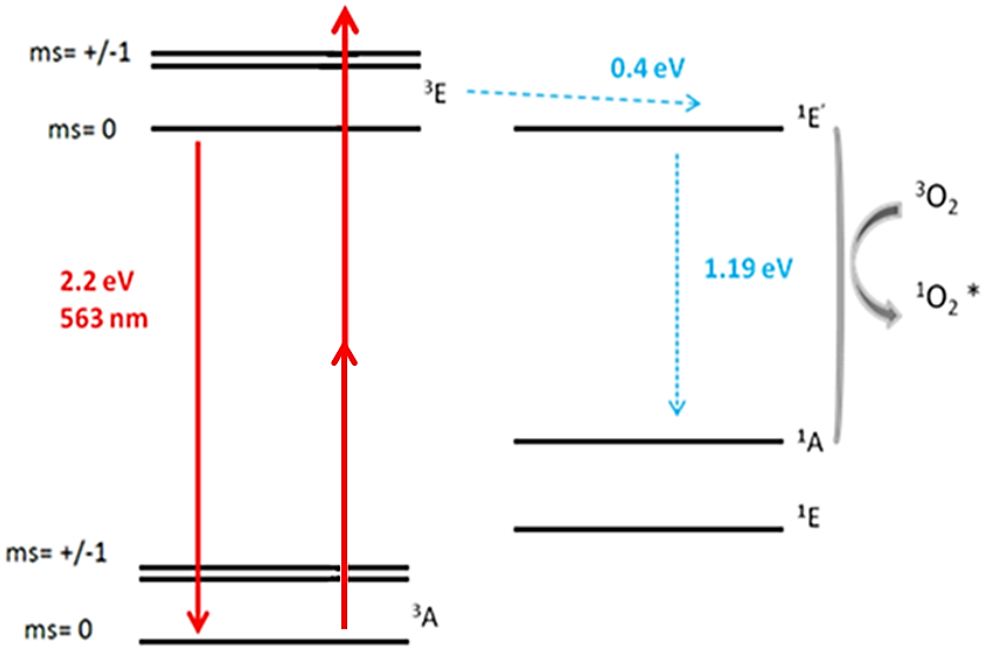

Figure S17. Energy-level diagram for NV^- centers.